

An impurity with a resonance in the vicinity of the Fermi energy

Mikhail Maslov,^{*} Mikhail Lemeshko,[†] and Artem G. Volosniev[‡]

IST Austria (Institute of Science and Technology Austria), Am Campus 1, 3400 Klosterneuburg, Austria

We study an impurity with a resonance level whose energy coincides with the Fermi energy of the surrounding Fermi gas. An impurity causes a rapid variation of the scattering phase shift for fermions at the Fermi surface, introducing a new characteristic length scale into the problem. We investigate manifestations of this length scale in the self-energy of the impurity and in the density of the bath. Our calculations reveal a model-independent deformation of the density of the Fermi gas, which is determined by the width of the resonance. To provide a broader picture, we investigate time evolution of the density in quench dynamics, and study the behavior of the system at finite temperatures. Finally, we briefly discuss implications of our findings for the Fermi-polaron problem.

I. INTRODUCTION

Systems with defects and impurities are ubiquitous in modern condensed matter physics [1–3]. Already simple impurity models such as a potential interacting with a continuum of states have led to a number of important discoveries, such as Friedel oscillations [4]. These simple models usually have a single length scale, e.g., the range of the potential, and are not able to describe an impurity whose structure introduces other length scales. For example the Kondo model [5] (and the Anderson model [6]) enjoys a relevant length scale defined by the Kondo temperature. Such additional length scales are often crucial for understanding the physics of realistic systems.

A basic impurity model with an additional length scale is the Friedel impurity with the resonance at the Fermi level. In spite of its simplicity, numerical analysis shows that real-space properties of that model have some similarities to those of the Kondo model [7, 8] whose understanding represents a milestone in condensed matter physics [9, 10]. Motivated by these numerical findings, we discuss here an analytically tractable model of an impurity that also features a resonance at the Fermi level. We discuss how the resonance affects properties of the Fermi gas, in particular the self-energy of the impurity, and the density profile of the Fermi gas. These results provide an illustration of how the width of the resonance introduces a length scale, which governs the physics at intermediate distances.

We formulate the problem such that our results can be tested in cold-atom systems. In particular, we assume a continuous homogeneous Fermi gas with the impurity that can either be an external potential or a tightly trapped atom. In the latter case, the resonance can be a Feshbach resonance [11] whose width is much smaller than the Fermi energy. For example, the typical Fermi temperature in experiments with ultracold ${}^6\text{Li}$ atoms is about 1 μK (see, e.g., [12], and references therein), which means that narrow resonances whose width is about

0.2 G [13, 14] satisfy the condition.

The paper is organized as follows. In Sec. II, we formulate the problem and introduce a simple model of an impurity with a Breit-Wigner resonant cross section [15] (see also [16]). Such a model allows us to calculate many-body properties of the system analytically. In Sec. III, we calculate the self-energy of the impurity in a Fermi gas using Fumi’s theorem [17]. In Sec. IV, we calculate the density of the fermionic bath, which is determined by the properties of the resonance. In Sec. V, we study time evolution of the density in a numerical quench experiment. In Sec. VI, we calculate finite-temperature properties of the system. In Sec. VII, we briefly explain implications of our findings for the Fermi-polaron problem. In Sec. VIII, we summarize our findings and give an outlook.

II. MODEL OF AN IMPURITY WITH A RESONANCE

We consider a heavy impurity immersed in an ideal Fermi gas. The Hamiltonian of the system in the coordinate representation reads

$$\hat{\mathcal{H}} = -\frac{\hbar^2}{2m} \sum_{i=1}^N \Delta_i + \sum_{i=1}^N U(\mathbf{r}_i), \quad (1)$$

where Δ_i and \mathbf{r}_i denote respectively the Laplacian and the coordinate of the i th fermion, m is the mass of a fermion, N is the number of particles in the bath, and U is the impurity-fermion interaction potential. Without loss of generality, we assume that the system is confined in a three dimensional box of size R with periodic boundary conditions, and use the system of units in which $\hbar \equiv 1$ and $m \equiv 1/2$.

The ground state of Hamiltonian (1) is the Slater determinant $\Psi(\mathbf{r}_1, \dots, \mathbf{r}_N) = (N!)^{-1/2} \det[\psi_j(\mathbf{r}_i)]_{i,j \leq N}$ over single-body wave functions $\psi_j(\mathbf{r}_i)$ that satisfy the Schrödinger equation

$$-\Delta_i \psi_j(\mathbf{r}_i) + U(\mathbf{r}_i) \psi_j(\mathbf{r}_i) = \varepsilon_j \psi_j(\mathbf{r}_i), \quad (2)$$

where ε_j denotes the energy of the j th fermionic state. Note that the subscript i will not carry any important information, so we omit it when possible.

^{*} mikhail.maslov@ist.ac.at

[†] mikhail.lemeshko@ist.ac.at

[‡] artem.volosniev@ist.ac.at

For later convenience, we introduce the Fermi energy of the bath as

$$\varepsilon_F \equiv \max(\varepsilon_j)_{j \leq N}. \quad (3)$$

The Fermi momentum, k_F , is defined via $k_F^2 \equiv \varepsilon_F$. k_F and ε_F set the length and energy scales in our problem. To illustrate our findings, we shall plot dimensionless quantities that correspond to the system of units in which $k_F = 1$.

Further analysis of the problem depends on the definition of the interaction U , which incorporates information about the internal structure of the impurity. We focus on the s -wave interaction and assume that there is no interaction in the higher partial waves – this is a standard approximation for cold-atom systems. In other words, we assume that the impurity-fermion interaction is radial $U(\mathbf{r}) \equiv U(r)$ and acts only on the wave functions with zero angular momentum. This assumption allows us to work with the s -wave radial Schrödinger equation

$$-\frac{d^2}{dr^2}\phi_j(r) + U(r)\phi_j(r) = k_j^2\phi_j(r), \quad (4)$$

where $\phi_j(r) \equiv r\psi_{s,j}(r)$ [$\psi_{s,j}(r)$ is $\psi_j(\mathbf{r})$ for s waves]. The momentum of a fermion, k_j , is defined via $k_j^2 \equiv \varepsilon_j$.

Equation (4) is a textbook one-body problem. We are interested in the physics outside the range of the potential r_I . Therefore, it is natural to define $U(r)$ through its scattering properties, namely the *phase shift* $\delta(k)$, which defines the solution $\phi_j(r)$ at $r > r_I$ [18]

$$\phi_j(r > r_I) = \gamma_j \sin(k_j r + \delta(k_j)), \quad (5)$$

where γ_j are the normalization coefficients. Equation (5) is a linear combination of the solutions to Eq. (4) with $U(r) = 0$. Without the impurity only the regular solution is possible, i.e., $\delta(k) \equiv 0$. The presence of the impurity induces a non-zero phase shift, which contains information about the impurity.

We use a simple model of an impurity with a *resonant* scattering phase shift. Namely, we consider $\delta_{\text{res}}(k)$ of the following form [18]

$$\delta_{\text{res}}(k) = \delta_0(k) + \text{atan}\left(\frac{k^2 - k_R^2}{\Gamma}\right) + \frac{\pi}{2}, \quad (6)$$

where Γ is the characteristic width of the resonance and k_R is the resonant momentum. Such a phase shift exhibits an abrupt change by π at the vicinity of the critical point $k \approx k_R$ (see the inset of Fig. 1). To simplify the analytical calculations in the following sections, we also introduce the approximation $\delta_{\text{res}}^*(k)$ to the phase shift (6) that is accurate for narrow resonances ($\Gamma \rightarrow 0$)

$$\delta_{\text{res}}(k) \approx \delta_{\text{res}}^*(k) = \delta_0(k) + \text{atan}\left(\frac{k - k_R}{\omega/2}\right) + \frac{\pi}{2}, \quad (7)$$

where $\omega \equiv \Gamma/k_R$.

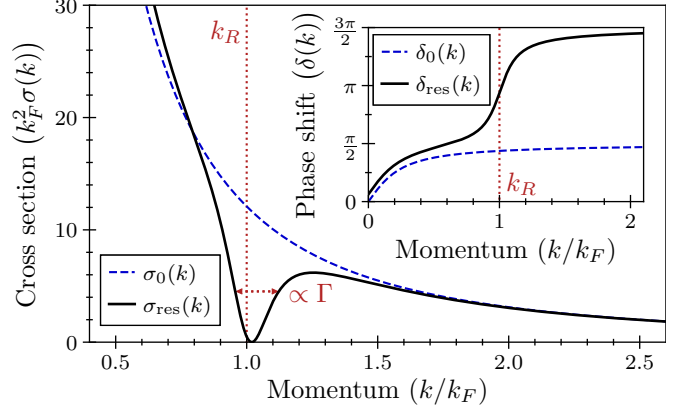


FIG. 1. (main panel) The black solid curve illustrates the dependence of the scattering cross section $\sigma_{\text{res}}(k)$ on the momentum k , see Eq. (9). The cross section exhibits a resonance at $k \approx k_R$ (dotted vertical line). The width of the resonance is determined by Γ . For comparison, we also plot $\sigma_0(k) = \frac{4\pi}{k^2} \sin^2(\delta_0(k))$ as a blue dashed curve. (inset) The scattering phase shift as a function of the momentum. Note that $\delta_{\text{res}}(k)$ changes rapidly in the vicinity of the resonance. Far from the resonance, both the phase shift and the cross section are determined by $\delta_0(k)$. We assume strong background interaction with $k_F\alpha = -5$. We fix the other parameters as $\Gamma = 0.2\varepsilon_F$, and $k_R = k_F$.

The precise form of $\delta_0(k)$ is not important for our analysis, as long as it does not change rapidly as a function of k . For the sake of discussion, we use

$$\delta_0(k) \equiv -\text{atan}(ka), \quad (8)$$

where α is the scattering length. This form of phase shift is typical for low-energy scattering, in particular, it is the standard form for scattering of cold atoms [11]. However, even for cold atoms, when the width of a characteristic Feshbach resonance is much smaller than the Fermi energy, one needs to consider the non-trivial behavior of the phase shift as in Eq. (6), see [11]. In this paper, we assume that U does not support bound states, which implies that $\alpha < 0$.

The scattering cross section, $\sigma(k)$, for the fermion-impurity collision reads

$$\sigma_{\text{res}}(k) = \frac{4\pi}{k^2} \sin^2(\delta_{\text{res}}(k)). \quad (9)$$

It exhibits a resonance with a Breit-Wigner profile [15] (see Fig. 1). The value of the scattering length α defines whether σ_{res} exhibits a peak ($|k_F\alpha| \gg 1$) or a dip ($|k_F\alpha| \ll 1$) [18]. To illustrate our findings graphically, we shall use a large impurity-fermion scattering length, $k_F\alpha = -5$. This allows us to provide an insight into the near-to-the-unitarity regime, which is usually challenging from the theoretical point of view.

The main advantage of the simple interaction model presented above is that it allows us to access analytically the many-body properties of the system. Additionally,

the aforementioned model can be easily extended to impurities with a discrete internal spectrum with more than a single level. This said, present studies might be beneficial for the prospective research on an analogue of the angulon quasiparticle [19, 20] in a fermionic environment.

III. SELF-ENERGY OF THE IMPURITY

The standard starting point for an analysis of systems with impurities is a calculation of the energy spectrum. In particular, one is interested in the energy required to immerse an impurity in a Fermi gas. This quantity is often called the self-energy of the impurity, ε_I . It is defined as the difference between the ground-state energies of the bath with and without the impurity.

To calculate ε_I for our problem, we employ Fumi's theorem [2, 17]. It states that the self-energy in the thermodynamic limit is a simple integral that involves only the scattering phase shift $\delta(k)$

$$\varepsilon_I = -\frac{2}{\pi} \int_0^{k_F} k \delta(k) dk. \quad (10)$$

Note that the scattering phase shift is always positive in our model, see Fig. (1), which implies $\varepsilon_I < 0$.

For the non-resonant phase shift $\delta_0(k)$, the integral in Eq. (10) leads to a simple expression (cf. [21])

$$\varepsilon_{I,0} = -\frac{\varepsilon_F}{\pi} \left[y + (1+y^2) \left(\frac{\pi}{2} + \text{atan}(y) \right) \right], \quad (11)$$

where $y \equiv 1/(k_F \alpha)$.

In general, the integral in Eq. (10) leads to a cumbersome expression, which we do not present here. Instead, we calculate the self-energy numerically. In Fig. 2, we plot the dependence of $\varepsilon_{I,\text{res}}$ on the momentum k_R for different values of the width parameter Γ . For a resonance far outside the Fermi sphere ($k_R \gg k_F$), the energy converges to the non-resonant behavior, described by Eq. (11). If the resonance is present inside the Fermi sphere ($k_R < k_F$), impurity's self-energy is decreased compared to $\varepsilon_{I,0}$. This happens due to a rearrangement of the Fermi sea upon the introduction of an additional energy level. For $\Gamma \rightarrow 0$, this will lead to the energy $\varepsilon_{I,0} + k_R^2 - k_F^2$. For larger values of Γ this value is slightly modified as shown in Fig. 2.

This paper focuses on the regime with $k_R \approx k_F$, and $\Gamma \rightarrow 0$. To calculate the self-energy in this limit, we use the approximation to the phase shift $\delta_{\text{res}}^*(k)$ which leads to

$$\begin{aligned} \varepsilon_{I,\text{res}} \approx \varepsilon_{I,0} - \frac{\varepsilon_F}{2} + \frac{k_F \omega}{2\pi} - \frac{\varepsilon_F}{\pi} \text{atan} \left(\frac{k_F - k_R}{\omega/2} \right) \\ + \frac{i}{2\pi} \left[\chi_-^2 \ln \left(1 + \frac{k_F}{\chi_-} \right) - \chi_+^2 \ln \left(1 - \frac{k_F}{\chi_+} \right) \right], \quad (12) \end{aligned}$$

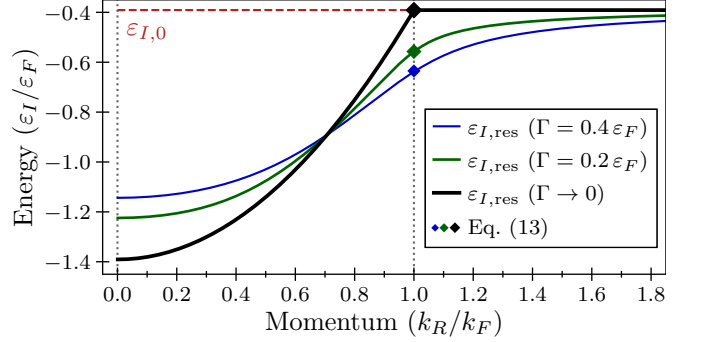


FIG. 2. The impurity self-energy $\varepsilon_{I,\text{res}}$ as a function of the position of the resonance, k_R (solid curves). For $k_R \gg k_F$, the energy of a system with a resonance converges to the value in Eq. (11), which is shown as a red dashed line. For $k_R \leq k_F$, the energy is decreased compared to $\varepsilon_{I,0}$, due to an extra energy level available for fermions. At $k_R = k_F$ the energy can be accurately approximated by Eq. (13) whose predictions are demonstrated by markers. We use $k_F \alpha = -5$.

where $\chi_{\pm} \equiv i\omega/2 \pm k_R$. Similar to Eq. (7), this approximation is accurate, when $\omega \rightarrow 0$. If the resonance is directly at the Fermi surface ($k_R = k_F$), the energy $\varepsilon_{I,\text{res}}$ is accurately approximated by (see the markers in Fig. 2)

$$\varepsilon_{I,\text{res}}|_{k_R \rightarrow k_F} \approx \varepsilon_{I,0} - \frac{\Gamma}{\pi} \ln \left(\frac{\Gamma}{e\varepsilon_F} \right), \quad (13)$$

which is non-analytical in Γ . The non-analytical behavior of the energy suggests the existence of a relevant length scale in addition to the one given by the density of the Fermi gas. This length scale should be proportional to $1/\Gamma$ as is evident from the argument of the logarithm in Eq. (13). For $\Gamma \rightarrow 0$, this length scale determines the physics of the system far outside the size of the potential. Therefore, the next step of our investigation is to consider the density profile of the Fermi gas.

IV. DENSITY OF THE FERMI GAS

The density of an ideal Fermi gas can be written as

$$n(r) = \rho_{l=0}(r) + \rho_{l>0}(r), \quad (14)$$

where $\rho_{l=0}(r) \equiv \rho(r)/r^2$ with $\rho(r) \equiv \sum_{i=1}^N |\phi_i(r)|^2$. The density $\rho_{l>0}(r)$ describes the density due to the higher angular momenta. It is not affected by the impurity, hence, we do not consider it from now on. In the thermodynamic limit, the summation over single-particle fermionic states can be replaced by the integration over momenta so that

$$\rho(r) = \frac{k_F}{\pi} - \frac{1}{\pi} \int_0^{k_F} \cos(2kr + 2\delta(k)) dk. \quad (15)$$

In the limit $r \rightarrow \infty$, the function $\cos(2kr + 2\delta(k))$ oscillates so rapidly that it contributes to the integration

only over an incomplete period directly at the Fermi surface. Therefore, for any scattering phase shift $\delta(k)$, we can write

$$\Delta\rho(r \rightarrow \infty) \rightarrow \Delta\rho_{\text{uni}}(k_F, r) \equiv -\frac{\sin(2k_F r + 2\delta(k_F))}{2r}, \quad (16)$$

where we define $\Delta\rho(r) \equiv \pi\rho(r) - k_F$. This universal behavior of the density function is called Friedel oscillations [4]. The Friedel oscillations were proven to be a powerful observable for the properties of a many-body environment, e.g., within quasiparticle interference technique [22–24], or the defect itself [25]. In this respect, any noticeable modification in the behavior of the density oscillations can be used as a probe of the system.

For impurities without any internal structure, the universal density profile of Eq. (16) describes the density well even in the vicinity of the impurity. However, the resonance can strongly affect the density, and additional terms should be added to Eq. (16) for a faithful description of the density profile close to the impurity. To understand this, note that one can use $\delta(k_F)$ in the argument of Eq. (15) only if $\delta(k_F) \simeq \delta(k_F + 1/r)$. With a resonance at the Fermi level, this condition can be satisfied only if $r \gg k_F/\Gamma$.

To illustrate this argument, we compute the density $\Delta\rho_{\text{res}}(r)$, see Fig. 3. Panel (a) shows the density for different values of k_R . We see that if k_R is far from k_F , i.e., $k_R^2 - k_F^2 > \Gamma$, the Friedel oscillations describe the density well for almost any value of r . However, if $k_R^2 - k_F^2 < \Gamma$, then the resonance energy level strongly modifies the density profile, see panel (b) for which $k_R = k_F$. Our conclusion here is that far from the impurity, the density always exhibits the Friedel oscillations. However, near the defect, the density can be non-trivially deformed.

The behavior of the density presented in Fig. 3 can be connected to node counting in Friedel's sum rule (for an introduction to the rule, see, e.g., [1]). If $k_R \gg k_F$, the number of full oscillations of the density within the range $r \in [r_I, R]$ should be equal to the number of fermions N in the bath. If the resonance lies inside the Fermi sea, the fermions “rearrange” and the number of nodes in $r \in [r_I, R]$ is $N - 1$. To illustrate this, we calculate the density, $\Delta\rho_{\text{res}}(r)$, for different values of k_R , see Fig. 3(a). The profile of the density reveals the deformation for $|k_F - k_R| < \sqrt{\Gamma}$, i.e., when the fermions at the Fermi level are coupled to the quasibound state.

To provide further analytical insight into the functional form of the density when $k_R \approx k_F$, we use the approximate form of the phase shift (7) with $\delta_0(k) \rightarrow \delta_F \equiv \delta_0(k_F)$. In what follows we also assume that $\delta_0(k_R) = \delta_0(k_F)$. Such a simplification allows us to approximate the density as follows

$$\Delta\rho_{\text{res}}(r) \approx \Delta\rho_{\text{def}}(r) - \Delta\rho_{\text{uni}}(k_F, r), \quad (17)$$

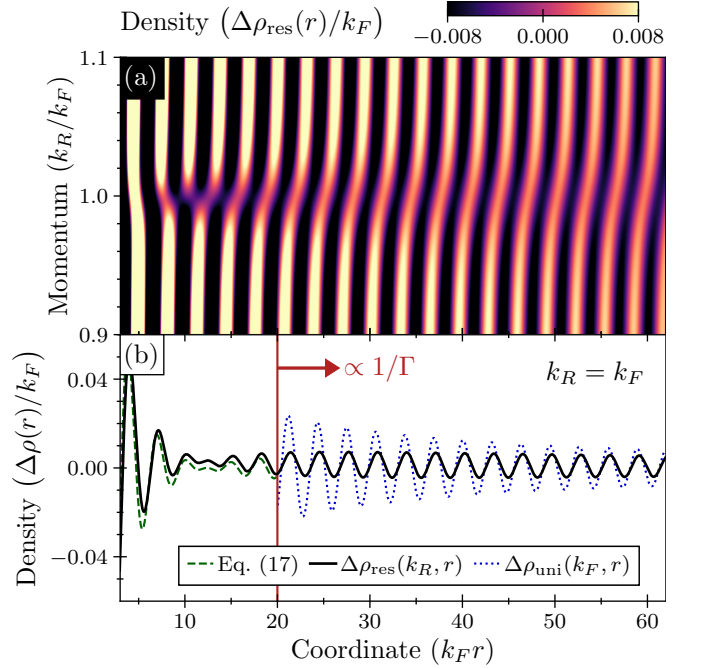


FIG. 3. (a) Dependence of the density function $\Delta\rho_{\text{res}}(r)$ on the resonance momentum k_R and coordinate r , calculated in finite system with $N = 1000$ fermions. Near the critical point $k_R \approx k_F$, the density is strongly modified, see the text for detail. (b) Density in the presence of an impurity with the resonant scattering phase shift $\delta_{\text{res}}(k)$ (black solid curve). The resonance is at the Fermi surface ($k_R = k_F$). Far from the impurity, density oscillations converge to the universal behavior (blue dotted curve). The oscillations close to the impurity ($r \lesssim 1/\Gamma$) can be approximated by the relation from Eq. (17) (green dashed). We use $k_F\alpha = -5$, $r_I = 0$ and $\Gamma = 0.05\epsilon_F$.

where

$$\begin{aligned} \Delta\rho_{\text{def}}(r) &= \omega e^{\omega r} \left[\cos(2k_R r + 2\delta_F) \text{Im}(\mathcal{J}_+(r)) \right. \\ &\quad \left. + \sin(2k_R r + 2\delta_F) \text{Re}(\mathcal{J}_-(r)) \right] \\ &\approx \omega e^{\omega r} \sin(2k_R r + 2\delta_F) \text{Ei}(-\omega r), \end{aligned} \quad (18)$$

and

$$\mathcal{J}_{\pm}(r) \equiv \mp \text{E}_1[-2i\chi_{\pm}r] - \text{E}_1[-2i(\chi_{\pm} - k_F)r], \quad (19)$$

where $\text{E}_1(z)$ is the generalization of the exponential integral $\text{Ei}(x)$ on the complex plane [26]. Approximation (17) is accurate when $\omega \rightarrow 0$, i.e., for narrow resonances, see Fig. 3(b). It reveals that the deformation of the many-body density function is induced by an effective interplay of the oscillations with periods given by k_R and k_F .

One can further use the asymptotic expansion of the exponential integral $\text{Ei}(-\omega r)$ for $r \rightarrow \infty$ to obtain the following expression

$$\Delta\rho_{\text{res}}(r) \approx -\frac{\sin(2k_F r + 2\delta_F)}{2r} + \frac{\sin(2k_R r + 2\delta_F)}{\omega r^2}. \quad (20)$$

This expression shows that the size of the deformed region is inversely proportional to the width parameter of the resonance Γ . For $r \gg k_R/\Gamma$, the second term becomes irrelevant and $\Delta\rho_{\text{res}}(r)$ converges to the universal Friedel oscillations (16). Note that the expression in Eq. (20) is universal, in a sense that it depends only on the parameters of the resonance, and not on the short-range physics.

To summarize this section: The width Γ introduces a relevant length scale, which leads to the density with two distinct patterns. As $r \rightarrow \infty$, the Friedel oscillations describe the density well. However, at distances $r \simeq k_R/\Gamma$, there is an additional oscillatory term in the density. The behavior that we observed has some similarities with those of the Kondo model where the extra length scale is given by the Kondo temperature, see also a similar observation in Ref. [8]. In particular, the charge density in the Kondo model features a crossover from short to long distances corresponding to the terms propositional to $1/r$ and $1/r^2$ in Eq. (20), which cannot be approximated by simple Friedel oscillations [27].

V. DYNAMICS UPON IMMERSION OF THE IMPURITY

So far we studied only the ground-state properties. Here, we focus on a corresponding time-dependent problem, which helps us to understand how the system reaches equilibrium following an immersion of the impurity. Investigation of quench dynamics is also a standard way to visualize relevant time scales in models with impurities.

Our protocol for studying quench dynamics is as follows: We assume that at $t < 0$ (t for time) there is no fermion-impurity interaction. At $t = 0$, the impurity-fermion interaction, $U(r)$, is turned on, which corresponds to the immersion of the defect into the bath. We analyze time evolution of the composite system at $t > 0$. As before, we focus only on the behavior of the s waves.

At $t = 0$, we write the wave function of the Fermi gas as the Slater determinant over the non-interacting functions $\phi_j^{(0)}(r) = \sqrt{2/R} \sin(\kappa_j r)$, where the momenta $\kappa_j \equiv \pi j/R$ are determined from the boundary condition $\phi_j^{(0)}(R) = 0$. In other words, we have

$$\Phi(r_1, \dots, r_N; t = 0) = \frac{1}{\sqrt{N!}} \det [\phi_j^{(0)}(r_i)]_{i,j \leq N}. \quad (21)$$

The corresponding density is

$$\rho_0(r) = \frac{2}{R} \sum_{i=1}^N \sin^2(\kappa_i r). \quad (22)$$

At $t > 0$, time evolution of the wave function $\Phi(r_1, \dots, r_N, t)$ formally can be written as

$$\Phi(r_1, \dots, r_N; t) = \exp(-i\hat{\mathcal{H}}_s t) \Phi_0(r_1, \dots, r_N; t = 0), \quad (23)$$

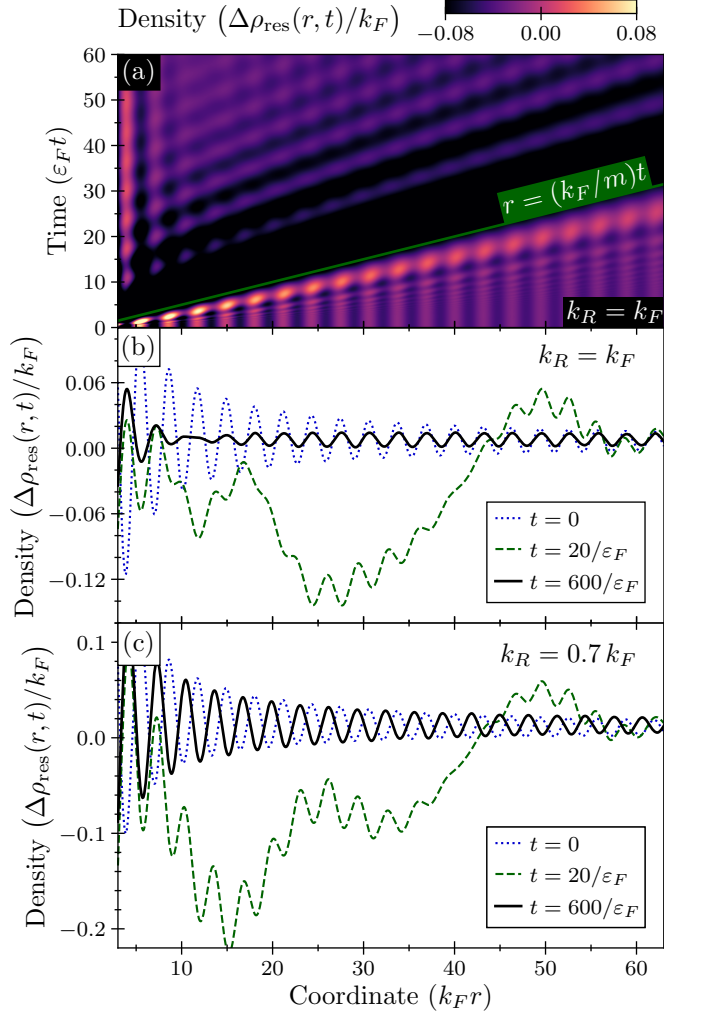


FIG. 4. (a) Time evolution of $\Delta\rho_{\text{res}}(r, t)$ with $k_R = k_F$ after a sudden immersion of the impurity at $t = 0$. The deformation of the density propagates with the group velocity k_F/m . (b,c) At large times ($t \rightarrow \infty$), the density converges to the ground-state result, discussed in Sec. IV. If $k_R = k_F$, the density oscillations are deformed (solid line) when compared to the universal Friedel oscillations (dotted line). The standard Friedel oscillations are realized with $k_R = 0.7 k_F$. In numerical simulations, we use $k_F\alpha = -5$, $r_I = 0$ and $\Gamma = 0.05 \varepsilon_F$.

where $\hat{\mathcal{H}}_s$ is the Hamiltonian of the s -wave part of the system. In order to simplify the evaluation of Eq. (23), the single-particle wave functions $\phi_j^{(0)}$ that enter Eq. (21) are expanded in the basis of one-body wave functions ϕ_j (see Eq. (4))

$$\phi_j^{(0)}(r_i) = \sum_{j'=1}^{\infty} A_{jj'} \phi_{j'}(r_i), \quad (24)$$

where the expansion coefficients are defined as

$$A_{jj'} = \int_0^R \phi_j^{(0)}(x) \phi_{j'}(x) dx. \quad (25)$$

The density at $t > 0$ can be written as

$$\rho(r, t) = \int \Phi^*(r, r_2, \dots, r_N, t) \Phi(r, r_2, \dots, r_N, t) dr_2 \dots dr_N \\ = \sum_{j=1}^N \left| \sum_{j'=1}^{\infty} \exp(-i\varepsilon_{j'} t) A_{jj'} \phi_{j'}(r) \right|^2. \quad (26)$$

We illustrate this density in Fig. 4 for a bath with $N = 300$, $R = \pi N/k_F$ and $k_R = k_F$. The momentum cutoff, which is required for the numerical evaluation of Eq. (26), is set to $k_\infty = 20k_F$. At $t > 0$, the density begins to deform. The deformation occurs in the light cone determined by the group velocity k_F/m (see Fig. 4(a)) – similar to the result of Ref. [28] without a resonance. Such a behavior is typical also for other models with impurities [29, 30].

Our numerical simulations do not show clear signs of a new time scale in the time dynamics of the density of the Fermi gas. The presence of the resonance is seen only in the long-time limit ($t \rightarrow \infty$), as exemplified in Fig. 4(b,c) for $t = 600/\varepsilon_F$. In particular, the oscillations of the density for $k_R = k_F$ are deformed in comparison to the Friedel oscillations that occur when the resonance is located far from the Fermi energy, e.g., at $k_R = 0.7k_F$. These results are in agreement with the ground-state calculations from the previous section.

VI. FINITE-TEMPERATURE PROPERTIES

Density oscillations due to the presence of the resonance can be observed experimentally. For example, in cold-atom systems, they could be detected either using another static impurity as a probe [31] or a quantum gas microscope [32]. To investigate the feasibility of such an observation, we should study the system at finite temperatures. Note that typical temperatures in current cold-atom experiments are $\tau \simeq 0.1$, where $\tau \equiv k_B T/\varepsilon_F$ and k_B is the Boltzmann constant, see [33] and references therein.

To describe a system in thermodynamic equilibrium at finite temperatures, we use the Fermi-Dirac distribution

$$n_{\text{FD}}(k, \tau) = \frac{1}{1 + \exp\left(\frac{k^2}{k_F^2 \tau} - \tilde{\mu}(\tau)\right)}, \quad (27)$$

where the chemical potential, $\tilde{\mu}(\tau) \equiv \mu/\varepsilon_F$, is given by [34]

$$\tilde{\mu}(\tau) = \tau \log\left(-\text{Li}_{3/2}^{-1}\left(-\frac{4}{3\sqrt{\pi}}\tau^{-3/2}\right)\right). \quad (28)$$

Here, $\text{Li}_{3/2}^{-1}(x)$ is the inverse of the polylogarithm function. At low temperatures ($\tau \ll 1$), one can use an approximate expression $\mu \simeq 1 - \pi^2 \tau^2 / 12$.

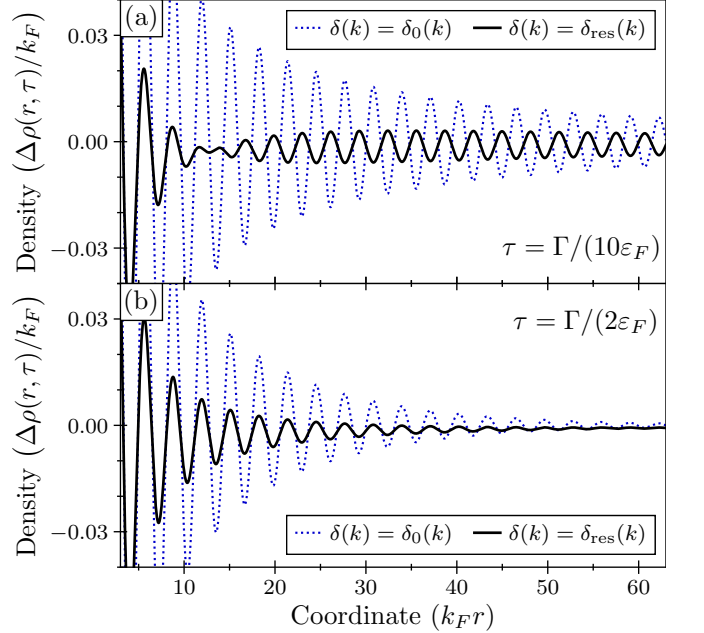


FIG. 5. The density $\Delta\rho(r, \tau)$ of the Fermi gas in the presence of the impurity with the resonant phase shift $\delta_{\text{res}}(k)$ (black solid) or with the phase shift $\delta_0(k)$ (blue dotted). We consider the resonance at the Fermi surface ($k_R = k_F$). (a) At temperatures much lower than Γ/k_B , the density is approximated by the ground-state result well. (b) At higher temperatures, the density is strongly affected by the temperature. We use $k_F \alpha = -5$ and $\Gamma = 0.05 \varepsilon_F$.

To study the effect of the temperature on the density, we consider the function

$$\Delta\rho(r, \tau) = \int_0^\infty \cos(2kr + 2\delta(k)) n_{\text{FD}}(k, \tau) dk, \quad (29)$$

which contains all information about the density oscillations. The dependence of $\Delta\rho(r, \tau)$ on the coordinate r is illustrated in Fig. 5. We assume $k_R = k_F$ and compare the density profiles with (solid curves) and without (dashed curves) a resonance. At temperatures significantly lower than Γ/k_B , e.g., at $\tau = \Gamma/(10\varepsilon_F)$, the ground-state result is accurate, see Fig. 5 (a) and Fig. 3. In contrast, at the temperatures comparable to the width of the resonance, e.g. $\tau = \Gamma/(2\varepsilon_F)$, the effect of the temperature is noticeable, see Fig. 5 (b), especially for a system with a resonance. In general, the difference between systems with and without a resonance becomes less prominent when increasing the temperature; it will disappear at temperatures $\tau \gg \Gamma/\varepsilon_F$. Indeed, the density oscillations are induced by the sharp edge of the Fermi sphere; they disappear at higher temperatures when the energy distribution of fermions becomes more gradual. We conclude that the resonance introduces a temperature scale into the problem, and only if $\tau \lesssim \Gamma/\varepsilon_F$ one can clearly see the effect of the resonance. Assuming a narrow resonance, $\Gamma/\varepsilon_F \simeq 0.1$, this condition implies

that our findings are within reach of state-of-the-art cold-atom experiments.

It is worth noting that one can also calculate the self-energy of the impurity $\varepsilon_I(\tau)$ at finite temperatures. To this end, one should use the extended version of Fumi's theorem (cf. [35])

$$\varepsilon_I(\tau) = -\frac{2}{\pi} \int_0^\infty k \delta(k) n_{\text{FD}}(k, \tau) dk. \quad (30)$$

For the temperatures of our interest ($\tau \lesssim 0.1$), Eq. (30) does not produce values significantly different from Eq. (10). This is expected: the energy is not sensitive to weak thermal perturbations at the surface of the Fermi sphere. Therefore, we refrain from discussing the self-energy of the impurity at finite temperatures further.

VII. IMPLICATIONS FOR THE FERMI POLARON

Finally, we use our findings in the context of another important model in cold-atom physics – the Fermi polaron [21, 36, 37], which is a quasiparticle introduced to describe experiments with two-component Fermi gases that have large (quasi)-spin imbalance [38–41] (for review, see Refs. [42, 43]). First of all, it is clear that our results cannot be easily extended to describe the residue or long-range spatial profile (e.g., the impurity-fermion correlation function) of the Fermi polaron. These properties are non-analytical in the mass of the impurity. In particular, they acquire important logarithmic corrections for large masses, see, e.g., Ref. [44]. By contrast, the self-energy is not expected to drastically change for the impurity with a finite mass [21]. Here, we estimate this energy using our results for a static impurity. For a different perspective on Fermi polarons near narrow Feshbach resonances, see Refs. [45–47].

The Hamiltonian of a mobile impurity in a Fermi gas is similar to Eq. (1) and reads

$$\hat{\mathcal{H}}_{\text{pol}} = -\frac{\hbar^2}{2M} \Delta_0 - \frac{\hbar^2}{2m} \sum_{i=1}^N \Delta_i + \sum_{i=1}^N U(\mathbf{r}_i - \mathbf{r}_0), \quad (31)$$

where the subscript 0 refers to the impurity with mass M . As in Sec. II, we assume periodic boundary conditions at $|\mathbf{r}| = R$, and work in a system of units with $m \equiv 1/2$ and $\hbar \equiv 1$.

To study the Hamiltonian (31), we first note that its eigenstates can be written as

$$\Psi(\mathbf{r}_0, \dots, \mathbf{r}_N) = \sum_{\mathbf{k}_0, \dots, \mathbf{k}_N} A(\mathbf{k}_0, \dots, \mathbf{k}_N) \prod_{j=0}^N e^{-i\mathbf{k}_j \cdot \mathbf{r}_j}, \quad (32)$$

where the wave vectors are quantized as $\mathbf{k} = \pi \mathbf{n}/R$ with integers $\mathbf{n} \equiv \{n_x, n_y, n_z\}$. The potential $\sum_{i=1}^N U(\mathbf{z}_i)$ depends only on the relative coordinates $\mathbf{z}_i \equiv \mathbf{r}_i - \mathbf{r}_0$,

which means that the total momentum of the system, $\mathbf{Q} \equiv \sum_{i=0}^N \mathbf{k}_i$, is conserved. This conservation implies that the wave function can be written as

$$\Psi(\mathbf{r}_0, \dots, \mathbf{r}_N) = e^{-i\mathbf{Q} \cdot \mathbf{r}_0} \Phi(\mathbf{z}_1, \dots, \mathbf{z}_N). \quad (33)$$

This observation motivates the use of the Lee-Low-Pines transformation [48] in coordinate space: $\hat{\mathcal{H}}'_{\text{pol}} \rightarrow e^{i\mathbf{Q} \cdot \mathbf{r}_0} \hat{\mathcal{H}}_{\text{pol}} e^{-i\mathbf{Q} \cdot \mathbf{r}_0}$, which removes the coordinate of the impurity from the Hamiltonian.

For the ground-state manifold ($\mathbf{Q} = 0$), we derive

$$\hat{\mathcal{H}}'_{\text{pol}} = -\sum_{i=1}^N \frac{\partial^2}{\partial \mathbf{z}_i^2} - \frac{1}{2M} \left(\sum_{i=1}^N \frac{\partial}{\partial \mathbf{z}_i} \right)^2 + \sum_{i=1}^N U(\mathbf{z}_i). \quad (34)$$

This Hamiltonian describes a complicated many-body problem where the particle-particle interactions are hidden in the mixed derivatives. To solve the problem, we use the following strategy: we assume that M is large, and write $\hat{\mathcal{H}}'_{\text{pol}} = \hat{\mathcal{H}}_0 + \hat{\mathcal{H}}_P$, where the leading part of the Hamiltonian is

$$\hat{\mathcal{H}}_0 = -\frac{1}{2\mu} \sum_{i=1}^N \frac{\partial^2}{\partial \mathbf{z}_i^2} + \sum_{i=1}^N U(\mathbf{z}_i), \quad (35)$$

with the reduced mass $\mu \equiv M/(1+2M)$. The perturbative term reads

$$\hat{\mathcal{H}}_P = -\frac{1}{2M} \sum_{i,j=1}^N \frac{\partial}{\partial \mathbf{z}_i} \frac{\partial}{\partial \mathbf{z}_j}. \quad (36)$$

As shown in App. A, this approach is related to the mean-field approximation.

The Hamiltonian (35) describes fermions with the mass μ interacting with a heavy impurity – a system discussed in detail in previous sections. The leading part of the Hamiltonian $\hat{\mathcal{H}}_0$ allows us to estimate the energy of the Fermi polaron using Fumi's theorem (compare to Sec. III)

$$\varepsilon_{\text{pol},0} \equiv \left\langle \hat{\mathcal{H}}_0 - \hat{\mathcal{H}}_0[U=0] \right\rangle = \frac{m}{\mu} \varepsilon_{I,\text{res}}. \quad (37)$$

The expectation value here is defined as

$$\left\langle \hat{O} \right\rangle \equiv \int \Phi^*(\mathbf{z}_1, \dots, \mathbf{z}_N) \hat{O} \Phi(\mathbf{z}_1, \dots, \mathbf{z}_N) d\mathbf{z}_1, \dots, d\mathbf{z}_N, \quad (38)$$

where the function Φ describes the ground state of the Hamiltonian $\hat{\mathcal{H}}_0$. The contribution from $\hat{\mathcal{H}}_P$ can be estimated within the first-order perturbation theory as follows

$$\varepsilon_{\text{pol},P} = \varepsilon_{\text{pol},0} + \left\langle \hat{\mathcal{H}}_P - \hat{\mathcal{H}}_P(U(\mathbf{z}_i) \equiv 0) \right\rangle. \quad (39)$$

This expression has a closed analytical form, which allows for a straightforward evaluation of the self-energy.

In Fig. 6(a), we compare the self-energies with and without the perturbative correction (i.e., $\varepsilon_{\text{pol},P}$ and

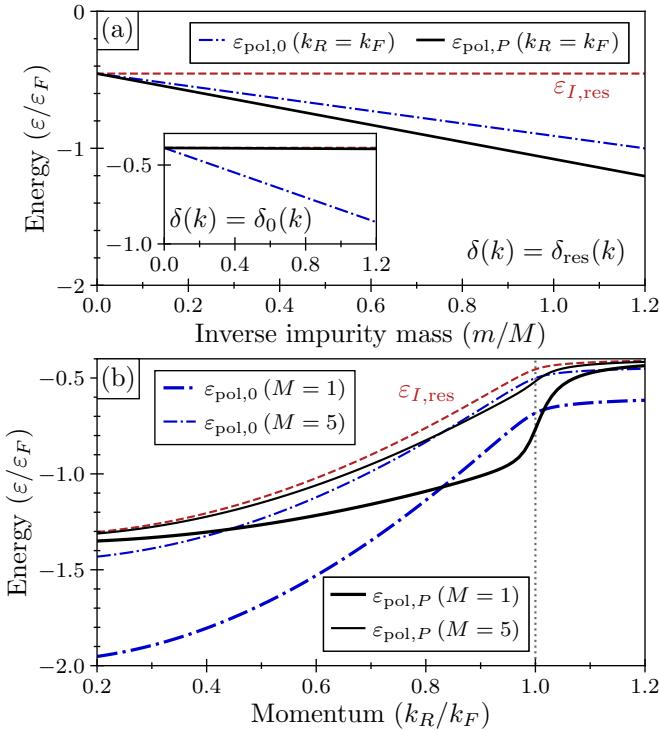


FIG. 6. (a) Dependence of the self-energy ε_{pol} on the inverse impurity mass M^{-1} . We assume that $k_R = k_F$. In the inset, we plot the self-energy of an impurity without a resonant level, see the phase shift in Eq. (8). (b) Dependence of the self-energy ε_{pol} on the position of the resonance k_R for small ($M = 1$, thick curve) and large ($M = 5$, thin curve) masses of the impurity. In both panels, $\varepsilon_{\text{pol},P}$ are shown as black solid curves, $\varepsilon_{\text{pol},0}$ are presented as dash-dotted curves. The self-energies of a heavy impurity are shown as red dashed curves. We use $k_F\alpha = -5$, $N = 300$ and $\Gamma = 0.05 \varepsilon_F$.

$\varepsilon_{\text{pol},0}$) to the self-energy of a heavy impurity $\varepsilon_{I,\text{res}}$. We consider the resonant phase shift from Eq. (6) with $k_R = k_F$. Akin to analytical results of Ref. [21], the self-energies are inversely proportional to the impurity mass M . Note however that without a resonance the dependence on the mass is very weak. The self-energy $\varepsilon_{\text{pol},P}$ is almost identical to the energy of a heavy impurity, see the inset of Fig. 6(a). This observation is in agreement with numerical results of Ref. [21]. A strong dependence on the mass is a direct consequence of the presence of a resonance. In Fig. 6(b), we illustrate this further by plotting the dependence of the polaron energy ε_{pol} on the resonance momentum k_R . We see a strong effect of the mass of the impurity only if the resonance is in the vicinity of the Fermi energy.

VIII. CONCLUSIONS AND OUTLOOK

We considered a three-dimensional fermionic bath in the presence of a static impurity with a resonance at the Fermi energy. Assuming the Breit-Wigner form of the

resonance, we computed several properties of the system. First, we calculated its self-energy using Fumi's theorem. The self-energy is non-analytic in the width of the resonance, which allowed us to suggest an existence of a length scale that determines the physics at intermediate ranges. To investigate this length scale further, we calculated the density of the Fermi gas. The oscillations of the density exhibit universal long-range physics beyond the standard Friedel oscillations, which can be intuitively explained in terms of a tunneling of a fermion to the internal state of the impurity. We argued that the density oscillations can be observed in current cold-atom experiments provided that their temperatures are a fraction of the Fermi temperature.

Our findings pave a way for a number of future studies. First of all, the resonance should introduce an additional time scale. We did not observe this scale in the quench dynamics of the density, but it must be important in the long-time dynamics of other observables. For example, the Anderson orthogonality catastrophe [49] manifests itself as a decay of a time-dependent overlap [50, 51], see Ref. [52] for review. The rate of this decay is usually given by the value of the phase shift at the Fermi energy. Fast change of the phase shift due to a resonance at the Fermi surface will introduce a new time scale into this problem. The importance of this scale should be investigated in a future work.

Second, the density of the Fermi gas dictates the shape of the induced impurity-impurity interactions, at least for weakly interacting heavy impurities. Our study suggests a possibility to strongly modify the density of the bath using the internal structure of the impurity. This may extend the family of existing impurity-impurity interactions mediated by Fermi gases [53–60]. Although, our paper focuses on a three-dimensional system, it makes sense to study induced correlations in low-dimensional geometries where the effects of interactions are usually more pronounced. Even an experimental observation of the density oscillations will be easier in one dimension where their decay is slow in comparison to higher spatial dimensions.

ACKNOWLEDGEMENTS

M.L. acknowledges support by the Austrian Science Fund (FWF), under project No. P29902-N27, and by the European Research Council (ERC) Starting Grant No. 801770 (ANGULON). A.G.V. acknowledges support by European Union's Horizon 2020 research and innovation programme under the Marie Skłodowska-Curie Grant Agreement No. 754411.

Appendix A: A mean-field approach to the Fermi polaron.

Here, we provide an additional insight into Eq. (34). We consider a single Slater determinant of the fermionic bath in the form suggested in Ref. [61]:

$$F(\mathbf{r}_0, \dots, \mathbf{r}_N) = \frac{\exp[i\mathbf{Q} \cdot \mathbf{r}_0]}{\sqrt{N!}} \begin{vmatrix} f_1(\mathbf{z}_1) & \dots & f_1(\mathbf{z}_N) \\ \vdots & \ddots & \vdots \\ f_N(\mathbf{z}_N) & \dots & f_N(\mathbf{z}_N) \end{vmatrix}, \quad (\text{A1})$$

where \mathbf{Q} is the momentum of the impurity, and f_i are functions that should be obtained variationally. The pre-factor $\exp[i\mathbf{Q} \cdot \mathbf{r}_0]$ together with the coordinate shift $\mathbf{z}_i \equiv \mathbf{r}_i - \mathbf{r}_0$ is motivated by the Lee-Low-Pines transformation [48]. Note that this mean-field approximation is similar in spirit to the ansatz proposed by Eugene Gross for the Bose gases [62], and which was successfully used for a Bose polaron in one [63–67] as well as in three spatial dimensions [68–71]. However, there is an important difference in the resulting calculations. Namely, one cannot neglect the term with mixed derivatives when calculating the energy of the Fermi gas, see the equation below. This difference significantly complicates the analysis of the Fermi polaron using the mean-field approximation, although it can still be analytically solvable for one-dimensional problems with a contact interaction [61].

The mean-field energy of the system is given by the

expectation value of the Hamiltonian (31)

$$\begin{aligned} \varepsilon = \int d\mathbf{r}_0 \dots d\mathbf{r}_N F(\mathbf{r}_0 \dots \mathbf{r}_N) \mathcal{H} F(\mathbf{r}_0 \dots \mathbf{r}_N) = \\ - \frac{1}{2\mu_M} \sum_{j=1}^N \left\langle \frac{\partial^2}{\partial \mathbf{z}^2} \right\rangle_{jj} + \sum_{j=1}^N \langle U(\mathbf{z}) \rangle_{jj} + \frac{1}{2M} \\ \times \left(\left[\mathbf{Q} + i \sum_{j=1}^N \left\langle \frac{\partial}{\partial \mathbf{z}} \right\rangle_{jj} \right]^2 - \sum_{j,k=1}^N \left\langle \frac{\partial}{\partial \mathbf{z}} \right\rangle_{jk} \left\langle \frac{\partial}{\partial \mathbf{z}} \right\rangle_{kj} \right), \end{aligned} \quad (\text{A2})$$

where we have defined

$$\langle O(\mathbf{z}) \rangle_{jk} \equiv \int f_j^*(\mathbf{z}) O(\mathbf{z}) f_k(\mathbf{z}) d\mathbf{z}. \quad (\text{A3})$$

We consider the ground state of the Fermi polaron ($\mathbf{Q} = 0$) and a limit of a heavy impurity ($M \gg m$). To find the set $\{f_i\}$ that minimizes the expectation value ε , we can follow an iterative procedure, where first we remove the last term in Eq. (A2), which is equivalent to minimizing \mathcal{H}_0 from the main text. Calculation of a correction due to the last term is then equivalent to calculating first order perturbation to the energy due to \mathcal{H}_P . Therefore, our approach to the problem can be seen as a mean-field approximation in the frame co-moving with the impurity, at least for a heavy impurity. Note that although we focus here on the ground-state properties in the present paper, future studies might employ the same approach to study excited states at $\mathbf{Q} \neq 0$.

[1] P. Coleman, *Introduction to many-body physics* (Cambridge University Press, 2015).

[2] G. D. Mahan, *Many-particle physics* (Springer Science & Business Media, 2013).

[3] A. Altland and B. D. Simons, *Condensed matter field theory* (Cambridge university press, 2010).

[4] J. Friedel, Metallic alloys, II Nuovo Cimento (1955-1965) **7**, 287 (1958).

[5] N. Andrei, K. Furuya, and J. Lowenstein, Solution of the kondo problem, Rev. Mod. Phys. **55**, 331 (1983).

[6] P. W. Anderson, Localized magnetic states in metals, Phys. Rev. **124**, 41 (1961).

[7] G. Bergmann, Friedel oscillations near kondo impurities: A comparison of numerical calculation methods, Phys. Rev. B **78**, 195124 (2008).

[8] Y. Tao and G. Bergmann, Friedel oscillation about a friedel-anderson impurity, Eur. Phys. J. B **85**, 42 (2012).

[9] I. Affleck, The kondo screening cloud: What it is and how to observe it, in *Perspectives of Mesoscopic Physics* (2010) pp. 1–44.

[10] I. V. Borzenets, J. Shim, and J. e. a. Chen, Observation of the kondo screening cloud, Nature **579**, 210–213 (2020).

[11] C. Chin, R. Grimm, P. Julienne, and E. Tiesinga, Feshbach resonances in ultracold gases, Rev. Mod. Phys. **82**, 1225 (2010).

[12] R. Grimm, Proceedings of the International School of Physics “Enrico Fermi” **164**, 413 (2007).

[13] K. E. Strecker, G. B. Partridge, and R. G. Hulet, Conversion of an atomic fermi gas to a long-lived molecular bose gas, Phys. Rev. Lett. **91**, 080406 (2003).

[14] C. H. Schunck, M. W. Zwierlein, C. A. Stan, S. M. F. Raupach, W. Ketterle, A. Simoni, E. Tiesinga, C. J. Williams, and P. S. Julienne, Feshbach resonances in fermionic ^6Li , Phys. Rev. A **71**, 045601 (2005).

[15] G. Breit and E. Wigner, Capture of slow neutrons, Phys. Rev. **49**, 519 (1936).

[16] U. Fano, Effects of configuration interaction on intensities and phase shifts, Phys. Rev. **124**, 1866 (1961).

[17] F. Fumi, Cxvi. vacancies in monovalent metals, The London, Edinburgh, and Dublin Philosophical Magazine and Journal of Science **46**, 1007 (1955).

[18] J. R. Taylor, *Scattering theory: the quantum theory of nonrelativistic collisions* (Courier Corporation, 2006).

[19] R. Schmidt and M. Lemeshko, Rotation of quantum impurities in the presence of a many-body environment, Physical review letters **114**, 203001 (2015).

[20] R. Schmidt and M. Lemeshko, Deformation of a quantum many-particle system by a rotating impurity, Physical Review X **6**, 011012 (2016).

[21] R. Combescot, A. Recati, C. Lobo, and F. Chevy, Normal state of highly polarized fermi gases: Simple many-body approaches, Phys. Rev. Lett. **98**, 180402 (2007).

[22] S. Grothe, S. Johnston, S. Chi, P. Dosanjh, S. A. Burke, and Y. Pennec, Quantifying many-body effects by high-resolution fourier transform scanning tunneling spectroscopy, *Phys. Rev. Lett.* **111**, 246804 (2013).

[23] L. Chen, P. Cheng, and K. Wu, Quasiparticle interference in unconventional 2d systems, *Journal of Physics: Condensed Matter* **29**, 103001 (2017).

[24] C. Dutreix, H. González-Herrero, I. Brihuega, M. I. Katsnelson, C. Chapelier, and V. T. Renard, Measuring the berry phase of graphene from wavefront dislocations in friedel oscillations, *Nature* **574**, 219 (2019).

[25] E. G. Dalla Torre, D. Benjamin, Y. He, D. Dentelski, and E. Demler, Friedel oscillations as a probe of fermionic quasiparticles, *Phys. Rev. B* **93**, 205117 (2016).

[26] M. Abramowitz and I. A. Stegun, *Handbook of mathematical functions with formulas, graphs, and mathematical tables*, Vol. 55 (US Government printing office, 1964).

[27] I. Affleck, L. Borda, and H. Saleur, Friedel oscillations and the kondo screening cloud, *Phys. Rev. B* **77**, 180404 (2008).

[28] J. M. Zhang and Y. Liu, Dynamical friedel oscillations of a fermi sea, *Phys. Rev. B* **97**, 075151 (2018).

[29] M. Medvedyeva, A. Hoffmann, and S. Kehrein, Spatiotemporal buildup of the kondo screening cloud, *Phys. Rev. B* **88**, 094306 (2013).

[30] B. Lechtenberg and F. B. Anders, Spatial and temporal propagation of kondo correlations, *Phys. Rev. B* **90**, 045117 (2014).

[31] A. Recati, J. N. Fuchs, C. S. Peça, and W. Zwerger, Casimir forces between defects in one-dimensional quantum liquids, *Phys. Rev. A* **72**, 023616 (2005).

[32] K. Riechers, K. Hueck, N. Luck, T. Lompe, and H. Moritz, Detecting friedel oscillations in ultracold fermi gases, *Eur. Phys. J. D* **71**, 232 (2017).

[33] S. Giorgini, L. P. Pitaevskii, and S. Stringari, Theory of ultracold atomic fermi gases, *Rev. Mod. Phys.* **80**, 1215 (2008).

[34] B. Cowan, On the chemical potential of ideal fermi and bose gases, *Journal of Low Temperature Physics* **197**, 412 (2019).

[35] W. E. Liu, Z.-Y. Shi, M. M. Parish, and J. Levinsen, Theory of radio-frequency spectroscopy of impurities in quantum gases, *Phys. Rev. A* **102**, 023304 (2020).

[36] F. Chevy, Universal phase diagram of a strongly interacting fermi gas with unbalanced spin populations, *Phys. Rev. A* **74**, 063628 (2006).

[37] N. Prokof'ev and B. Svistunov, Fermi-polaron problem: Diagrammatic monte carlo method for divergent sign-alternating series, *Phys. Rev. B* **77**, 020408 (2008).

[38] A. Schirotzek, C.-H. Wu, A. Sommer, and M. W. Zwierlein, Observation of fermi polarons in a tunable fermi liquid of ultracold atoms, *Phys. Rev. Lett.* **102**, 230402 (2009).

[39] M. Koschorreck, D. Pertot, E. Vogt, B. Fröhlich, M. Feld, and M. Köhl, Attractive and repulsive fermi polarons in two dimensions, *Nature* **485**, 619 (2012).

[40] M. Cetina, M. Jag, R. S. Lous, I. Fritzsche, J. T. Walraven, R. Grimm, J. Levinsen, M. M. Parish, R. Schmidt, M. Knap, *et al.*, Ultrafast many-body interferometry of impurities coupled to a fermi sea, *Science* **354**, 96 (2016).

[41] F. Scazza, G. Valtolina, P. Massignan, A. Recati, A. Amico, A. Burchianti, C. Fort, M. Inguscio, M. Zaccanti, and G. Roati, Repulsive fermi polarons in a resonant mixture of ultracold ^6Li atoms, *Phys. Rev. Lett.* **118**, 083602 (2017).

[42] P. Massignan, M. Zaccanti, and G. M. Bruun, Polarons, dressed molecules and itinerant ferromagnetism in ultracold fermi gases, *Reports on Progress in Physics* **77**, 034401 (2014).

[43] F. Chevy and C. Mora, Ultra-cold polarized fermi gases, *Reports on Progress in Physics* **73**, 112401 (2010).

[44] C. Trefzger and Y. Castin, Polaron residue and spatial structure in a fermi gas, *EPL* **101**, 30006 (2013).

[45] C. Trefzger and Y. Castin, Impurity in a fermi sea on a narrow feshbach resonance: A variational study of the polaronic and dimeronic branches, *Phys. Rev. A* **85**, 053612 (2012).

[46] P. Massignan, Polarons and dressed molecules near narrow feshbach resonances, *EPL (Europhysics Letters)* **98**, 10012 (2012).

[47] R. Qi and H. Zhai, Highly polarized fermi gases across a narrow feshbach resonance, *Phys. Rev. A* **85**, 041603 (2012).

[48] T. Lee, F. Low, and D. Pines, The motion of slow electrons in a polar crystal, *Physical Review* **90**, 297 (1953).

[49] P. W. Anderson, Infrared catastrophe in fermi gases with local scattering potentials, *Phys. Rev. Lett.* **18**, 1049 (1967).

[50] P. Nozières and C. T. De Dominicis, Singularities in the x-ray absorption and emission of metals. iii. one-body theory exact solution, *Phys. Rev.* **178**, 1097 (1969).

[51] N. Rivier and E. Simanek, Exact calculation of the orthogonality catastrophe in metals, *Phys. Rev. Lett.* **26**, 435 (1971).

[52] R. Schmidt, M. Knap, D. A. Ivanov, J.-S. You, M. Cetina, and E. Demler, Universal many-body response of heavy impurities coupled to a fermi sea: a review of recent progress, *Reports on Progress in Physics* **81**, 024401 (2018).

[53] J. N. Fuchs, A. Recati, and W. Zwerger, Oscillating casimir force between impurities in one-dimensional fermi liquids, *Phys. Rev. A* **75**, 043615 (2007).

[54] S. De and I. Spielman, Fermion-mediated long-range interactions between bosons stored in an optical lattice, *Applied Physics B* **114**, 527 (2014).

[55] M. Pasek and G. Orso, Induced pairing of fermionic impurities in a one-dimensional strongly correlated bose gas, *Phys. Rev. B* **100**, 245419 (2019).

[56] D. Huber, H.-W. Hammer, and A. G. Volosniev, In-medium bound states of two bosonic impurities in a one-dimensional fermi gas, *Phys. Rev. Research* **1**, 033177 (2019).

[57] T. Enss, B. Tran, M. Rautenberg, M. Gerken, E. Lippi, M. Drescher, B. Zhu, M. Weidmüller, and M. Salmhofer, Scattering of two heavy fermi polarons: Resonances and quasibound states, *Phys. Rev. A* **102**, 063321 (2020).

[58] J. Kwasniok, S. I. Mistakidis, and P. Schmelcher, Correlated dynamics of fermionic impurities induced by the counterflow of an ensemble of fermions, *Phys. Rev. A* **101**, 053619 (2020).

[59] B. J. DeSalvo, K. Patel, G. Cai, and C. Chin, Observation of fermion-mediated interactions between bosonic atoms, *Nature* **568**, 61 (2019).

[60] H. Edri, B. Raz, N. Matzliaf, N. Davidson, and R. Ozeri, Observation of spin-spin fermion-mediated interactions between ultracold bosons, *Phys. Rev. Lett.* **124**, 163401 (2020).

[61] D. Edwards, Magnetism in single-band modelsexact one-

dimensional wave functions generalised to higher dimensions, *Progress of Theoretical Physics Supplement* **101**, 453 (1990).

[62] E. Gross, Motion of foreign bodies in boson systems, *Annals of Physics* **19**, 234 (1962).

[63] A. G. Volosniev and H.-W. Hammer, Analytical approach to the bose-polaron problem in one dimension, *Phys. Rev. A* **96**, 031601 (2017).

[64] S. I. Mistakidis, A. G. Volosniev, N. T. Zinner, and P. Schmelcher, Effective approach to impurity dynamics in one-dimensional trapped bose gases, *Phys. Rev. A* **100**, 013619 (2019).

[65] G. Panochko and V. Pastukhov, Mean-field construction for spectrum of one-dimensional bose polaron, *Annals of Physics* **409**, 167933 (2019).

[66] J. Jager, R. Barnett, M. Will, and M. Fleischhauer, Strong-coupling bose polarons in one dimension: Condensate deformation and modified bogoliubov phonons, *Phys. Rev. Research* **2**, 033142 (2020).

[67] G. M. Koutentakis, S. I. Mistakidis, and P. Schmelcher, Pattern formation in one-dimensional polaron systems and temporal orthogonality catastrophe, arXiv e-prints , arXiv:2110.11165 (2021), arXiv:2110.11165 [cond-mat.quant-gas].

[68] N.-E. Guenther, R. Schmidt, G. M. Bruun, V. Gurarie, and P. Massignan, Mobile impurity in a bose-einstein condensate and the orthogonality catastrophe, *Phys. Rev. A* **103**, 013317 (2021).

[69] M. Drescher, M. Salmhofer, and T. Enss, Theory of a resonantly interacting impurity in a bose-einstein condensate, *Phys. Rev. Research* **2**, 032011 (2020).

[70] O. Hryhorchak, G. Panochko, and V. Pastukhov, Mean-field study of repulsive 2d and 3d bose polarons, *Journal of Physics B: Atomic, Molecular and Optical Physics* **53**, 205302 (2020).

[71] P. Massignan, N. Yegovtsev, and V. Gurarie, Universal aspects of a strongly interacting impurity in a dilute bose condensate, *Phys. Rev. Lett.* **126**, 123403 (2021).